Effect of low-level jet on turbine aerodynamic blade loading using large-eddy simulations

Effect of low-level jet on turbine aerodynamic blade loading using large-eddy simulations

Srinidhi N. Gadde, Luoqin Liu, & Richard J. A. M. Stevens

Physics of Fluids Group, Max Planck Center Twente for Complex Fluid Dynamics, J. M. Burgers Center for Fluid Dynamics and MESA+ Research Institute, University of Twente, P. O. Box 217, 7500 AE Enschede, The Netherlands

E-mail: s.nagaradagadde@utwente.nl; r.j.a.m.stevens@utwente.nl

Abstract. Low-level jets (LLJs) are winds with high-shear and large wind energy potential. We perform large-eddy simulations (LES) with actuator line modeling of a turbine operating in a moderately stable boundary layer in the presence of LLJs. We find that the turbine tip and root vortices break down quickly when the LLJ is above the turbine rotor swept area. In contrast, the wake recovery is slow, and the vortices are stable when the LLJ is in the middle or even below the rotor swept area. The LLJ shear causes significant azimuthal variation in the external aerodynamic blade loading, increasing fatigue loading on the turbines. We observe that both tangential and axial forces on the blades are highest when the blade directly interacts with the LLJ. Azimuthal variation in the tangential forces on the blades is the highest when the LLJ is above the rotor swept area, i.e. when the turbine operates in the positive shear region of LLJ, with the blade tip interacting with the LLJ.

1. Introduction

Wind turbine wakes and external aerodynamic blade loadings are significantly affected by the atmospheric boundary layer (ABL) shear and turbulence intensity [1]. For example, Chamorro and Porté-Agel [2] showed that both shear and turbulence in the boundary layer affect the turbine vortex structures. Bartl *et al.* [3] report that in the presence of shear the tip-vortex turbulent kinetic energy is higher in the upper part of the wake than in the lower part of the wake. Recently, Kleusberg *et al.* [4] report that shear affects the wake expansion above and below hub-height such that an asymmetric wake develops. The shear in the ABL also gives rise to changes in the azimuthal distribution of turbine axial and tangential forces [1]. Low-level jets (LLJs) are one of the most extreme shear events in the lowest 50 to 500 m of the atmosphere [5, 6]. They are generally observed in weak to moderately stable ABLs [7, 8]. Climatology of LLJs has been widely studied by field measurements [9, 10, 11, 12] and numerical computations [13, 14, 15]. The ever-increasing turbine height and diameters give rise to complex scenarios in which the turbines might be subjected to fatigue loading due to strong positive shear created by extreme shear events like LLJs. For taller turbines LLJ events

can create negative shear across the rotor plane resulting in complex loading scenarios and fatigue cycles [16]. Therefore, it is important to understand the turbine-shear interraction in the event of an LLJ.

Some aspects of the interaction between wind turbines and LLJs have been studied previously. For example, Lu and Porté-Agel [17] performed large-eddy simulations (LES) of an infinite wind farm in the presence of an LLJ and reported the formation of non-axisymmetric wakes and the elimination of the LLJ due to the mixing induced by the turbines. Bhaganagar and Debnath [18] studied cases in which the LLJ height is above or equal to the turbine hub-height. They report that the vertical shear of the LLJ causes an interaction between the root and lower tip vortices, which results in a root vortex instability enhancing shear stress and turbulent kinetic energy. Na *et al.* [19] and Gadde and Stevens [20] performed LES of wind farms and report higher vertical kinetic energy entrainment rates when the LLJ is above the wind farm. A recent wind farm study by Gadde and Stevens [21] reports that the interaction between the negative shear and velocity deficit in the wind turbine wake can generate an upward momentum flux, which is beneficial for the power production of downstream turbines when the LLJ is below the turbine hub-height.

Some previous studies found that LLJs increase the mechanical loads and fatigue experienced by the turbines [22]. Furthermore, Gutierrez *et al.* [23] performed structural analysis using the FAST (Fatigue, Aerodynamics, Structures, and Turbulence) code [24] and showed that the negative shear in the rotor swept area region reduces the loading on tower and nacelle, but the effect is marginal on the turbine blades. This is surprising as the LLJ shear is generally expected to induce higher loads on the blades. Furthermore, Gutierrez *et al.* [25] report asymmetric azimuthal variation of turbine tip deflection in the presence of an LLJ. Furhtermore, previous studies of LLJ-turbine interaction [17, 18] have not focused on the azimuthal and radial distribution of aerodynamic loads due to an LLJ. In this context, further analysis of the turbine wake and external aerodynamic blade loading increases our understanding of LLJ-turbine interaction. Therefore, in the present work, we use LES in combination with an actuator line model to study the external aerodynamic blade loading and wake vortex structures for three scenarios in which:

1. the LLJ is above the turbine hub-height ($z_{\text{jet}} > z_h$). In this case, the turbine operates in a turbulent, positive shear region.
2. the LLJ height is equal to the turbine hub-height ($z_{\text{jet}} \approx z_h$) due to which the turbine rotor experiences positive and negative shear below and above the hub-height.
3. the LLJ is below the turbine hub-height ($z_{\text{jet}} < z_h$), which means the turbine operates in a non-turbulent negative shear region.

2. Simulation methodology

In LES the large-scale flow structures are resolved and the effect of small-scale structures known as sub-grid scale eddies is modeled. We use an updated version of the code

developed by Albertson & Parlange [26, 27]. The code has been successfully used to simulate neutral and stable boundary layers [28, 20]. Here we like to mention that the anisotropic minimum dissipation (AMD) model [29] is used in this simulation. The governing equations are:

$$\partial_i \widetilde{u}_i = 0, \tag{1}$$

$$\begin{aligned}\partial_t \widetilde{u}_i + \partial_j \left(\widetilde{u}_i \widetilde{u}_j\right) = &-\partial_i \widetilde{p} - \partial_j \tau_{ij} + g\beta(\widetilde{\theta} - \widetilde{\theta}_0)\delta_{i3} \\ &+ f_c(U_g - \widetilde{u})\delta_{i2} - f_c(V_g - \widetilde{v})\delta_{i1} + \widetilde{f}_x \delta_{i1} + \widetilde{f}_y \delta_{i2},\end{aligned} \tag{2}$$

$$\partial_t \widetilde{\theta} + \widetilde{u}_j \partial_j \widetilde{\theta} = -\partial_j q_j, \tag{3}$$

here Δ represents a spectral cut-off filter with the tilde representing spatial filtering, $\widetilde{u}_i = (\widetilde{u}, \widetilde{v}, \widetilde{w})$ and $\widetilde{\theta}$ are the grid scale velocities and potential temperature, respectively, g is the acceleration due to gravity, $\beta = 1/\theta_0$ represents the buoyancy parameter with respect to the reference potential temperature θ_0, δ_{ij} is the Kronecker delta, and f_c represents the Coriolis parameter. The ABL is driven by the mean pressure p_∞, derived from the geostrophic wind with the equation, $U_g = -\frac{1}{\rho f_c}\frac{\partial p_\infty}{\partial y}$ and $V_g = \frac{1}{\rho f_c}\frac{\partial p_\infty}{\partial x}$ as its components. $\widetilde{p} = \widetilde{p}^*/\rho + \sigma_{kk}/3$ is the altered pressure, which is the sum of the trace of the SGS stress, $\sigma_{kk}/3$, and the kinematic pressure $\widetilde{p}^*/\rho$, where ρ is the density of the fluid. $\widetilde{f}_x$ and $\widetilde{f}_y$ represents the turbine forces which are modeled using the actuator line method [30, 1]. In the actuator line implementation in our code the point forces calculated on the actuator points are smeared on the background grid with a kernel of width $\epsilon = 2\Delta$ [31], where Δ represents the grid size in the streamwise direction. The actuator line model in the code has been extensively validated against wind tunnel experiments [32]. We use a standard pseudo-spectral method for discretization in the horizontal directions and central difference scheme in the vertical directions. The wall stresses and fluxes are modeled using the Monin-Obukhov similarity theory with the stability correction functions proposed by Beare *et al.* [33]. We refer to Gadde and Stevens [20] for detailed explanation of the numerical method and wall-stress modeling. Finally, we use concurrent-precursor method [34] to generate the incoming flow.

2.1. Boundary layer initialization

We simulate continuously turbulent moderately stable boundary layers (SBLs). The roughness lengths for momentum and heat fluxes are set to 0.002 m and 0.0002 m, respectively. We consider two cooling rates, i.e. 0.25 K $\cdot$ hour^{-1} (SBL–1) and 0.50 K $\cdot$ hour^{-1} (SBL–2), which generate a LLJ at 195 m and 140 m, respectively. The geostrophic forcing is set to $G = (9.0, 0.0)$ ms^{-1} and the Coriolis parameter is set to $f_c = 1.159 \times 10^{-4}$ s^{-1}, which corresponds to a latitude of 52.8° that is representative for the Dutch North Sea. The velocity is initialized with the geostrophic velocity and temperature is initialized with a constant temperature of 286 K. Uniform random perturbations are added to the initial profiles up to a height of 200 m to trigger turbulence. The boundary layer reaches a quasi-steady state at the end of 8$^{\text{th}}$ hour.

Effect of LLJ on aerodynamic blade loading using LES

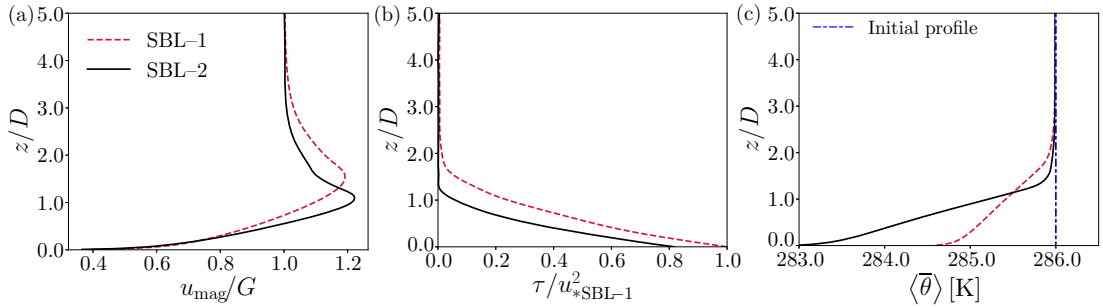

Figure 1: (a) Horizontal velocity magnitude, (b) the turbulent momentum flux, and (c) temperature profiles for SBL-1 and SBL-2, see table 1. The height is normalized with the turbine diameter D.

Table 1: C_r is the surface cooling rate, z_i is the boundary layer height, z_{jet} is the jet height, u_* is the friction velocity, u_{jet}/G is the non-dimensionalized jet velocity, and z_i/L represents the stability parameter, where L is the surface Obukhov length.

Case	C_r [$\mathrm{K \cdot h^{-1}}$]	z_i [m]	z_{jet} [m]	u_* [$\mathrm{ms^{-1}}$]	u_{jet}/G	z_i/L
SBL-1	0.25	194	195	0.228	1.19	1.72
SBL-2	0.50	132	140	0.206	1.22	2.48

In the simulations, we consider the National Renewable Energy Laboratory (NREL) 5 megawatt (MW) turbine with a diameter of $D = 126$ m. The computational domain is $24D \times 6D \times 6D$, which corresponds to 3.072 km $\times$ 0.768 km $\times$ 0.768 km in x-, y-, and z-directions, respectively. The turbine is located approximately $4D$ from the entrance of the computation domain. The domain is discretized by $1024 \times 384 \times 384$ grid points, i.e. the resolution of 3 m in x-direction and 2 m in the y- and z- directions. This ensures that there are 32 fluid points along each blade, which has been previously found to fulfill the basic demands of actuator line model LES [35].

The boundary layer characteristics are presented in Table 1. The boundary layer height is defined as the height at which the shear stress reaches 5% of its surface value [33]. The horizontal velocity profile $u_{\mathrm{mag}} = \left\langle \sqrt{\overline{u}^2 + \overline{v}^2} \right\rangle$, where $\overline{u}$ and $\overline{v}$ are the time-averaged streamwise and spanwise velocities, respectively and $\langle\rangle$ represents planar averaging, in Fig. 1(a) show a pronounced LLJ at heights of interest. Fig. 1(b) shows the horizontally averaged vertical momentum flux $\tau = \left\langle \sqrt{(\overline{u'w'})^2 + (\overline{v'w'})^2} \right\rangle$, where $\overline{u'w'} = (\overline{uw} + \overline{\tau_{xz}}) - \overline{u}\ \overline{w}$ and $\overline{v'w'} = (\overline{vw} + \overline{\tau_{yz}}) - \overline{v}\ \overline{w}$, which reveals that there is negligible turbulence above the jet. This lack of turbulence above the jet will have significant impact on the turbine wake evolution. A detailed discussion on the boundary layer characteristics can be found in Gadde & Stevens (2021b) [21]. We consider three turbine hub-height to jet height ratios (z_h/z_{jet}):

1. $z_h = 0.4 z_{\mathrm{jet}}$. This simulation is performed in SBL-1. The turbine operates

completely in a turbulent region.

2. $z_h = 1.0z_{\text{jet}}$. This simulation is performed in SBL-2, which is turbulent below hub-height with positive shear and turbulence above hub-height is limited with negative shear.
3. $z_h = 1.5z_{\text{jet}}$. This simulation is performed in SBL-2. The turbine operates completely in a region of negligible atmospheric turbulence with negative shear.

3. Results and discussion

3.1. Vorticity magnitude and wake turbulence

A visualization of the instantaneous vorticity magnitude Ω_{mag} for the three cases is presented in Fig. 2(a). We observe typical helical tips and root vortices behind the turbines. The most recognizable feature in the vorticity contours is that the stability of the root and tip vortices increases as the jet height decreases. Troldborg *et al.* [35] showed that the tip vortices break down immediately downstream of the turbine due to atmospheric turbulence. When $z_{\text{jet}} > z_h$, the turbine operates in a positive shear region with high atmospheric turbulence, due to which the tip and root vortices are weak. The figure shows that proximity to the ground also affects the breakdown of the vortices. When $z_{\text{jet}} \approx z_h$, pronounced tip and root vortices are formed, which start to become unstable approximately $2D$ downstream of the turbine. In contrast, for $z_{\text{jet}} < z_h$ the root and tip vortices are highly stable and only start to break down about $5D$ downstream of the turbine. The reason for this is that the turbine is operating in the non-turbulent region above the jet.

Wake turbulence is an important quantity as it directly affects the performance of downstream turbines [36]. Wake recovery primarily depends on the turbulence intensity and the atmospheric stability [37, 36]. LLJ maximum is generally found at the top of the SBL and the region above has high thermal stability and minimal turbulence intensity. It is also reported that in the event of an LLJ the atmosphere is generally stable and the turbulent kinetic energy levels are lower compared to an unstable or neutral boundary layer [12]. Figure 2(b) shows the streamwise turbulence intensity $\sigma_u = u'/u_{\text{hub}}$ at hub-height, where u' represents the fluctuating streamwise velocity. As is evident from the figure, the turbulence intensity in the wake is highest when the LLJ is above the turbine ($z_{\text{jet}} > z_h$). We observe that due to higher atmospheric turbulence in this region, the tip and root vortices become unstable and break down, expanding to the rest of the wake. For $z_{\text{jet}} \approx z_h$, the turbulence intensity is lower, and the non-turbulent wake region extends up to approximately $2D$ behind the turbine. This is consistent with the observation of stable tip and root vortices up to that location. However, when $z_{\text{jet}} < z_h$ the turbulence in the wake is very low up to $4D$ to $5D$ behind the turbine as the turbine operates in a thermally stratified flow region with limited turbulence. Again this observation is consistent with the observed stability of the tip and hub vortices up to $5D$ downstream of the turbine.

Effect of LLJ on aerodynamic blade loading using LES

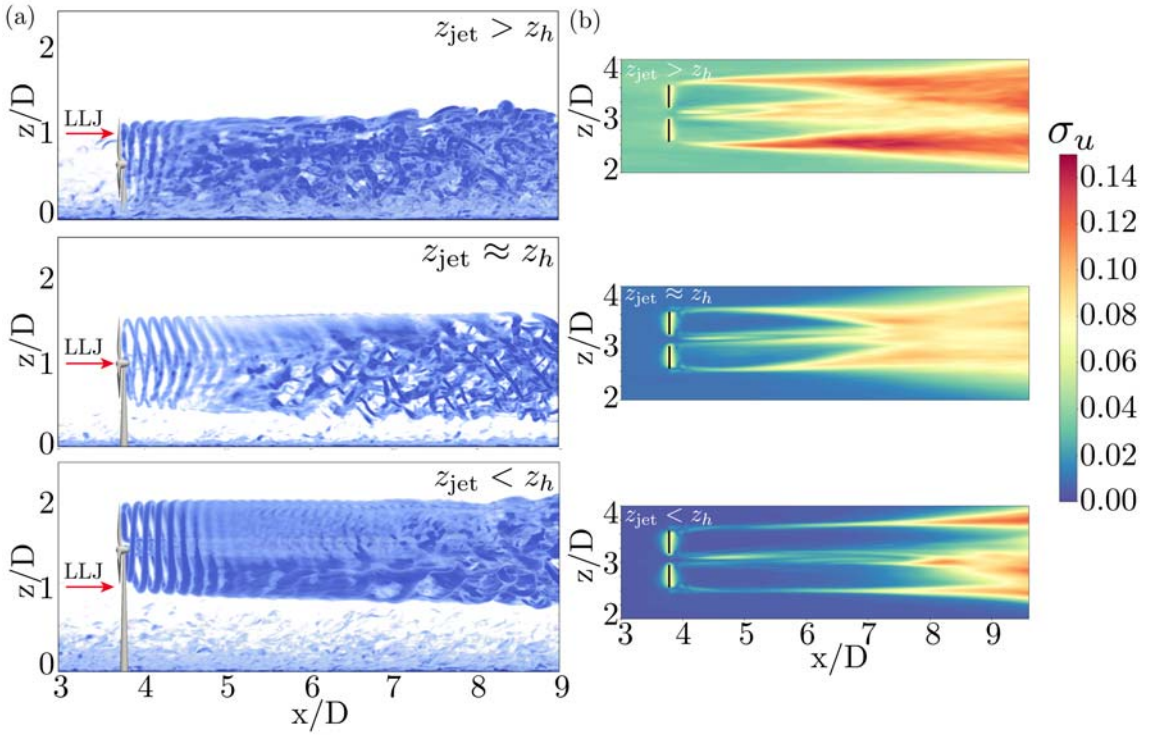

Figure 2: (a) Visualization of vorticity magnitude Ω_{mag} for three different scenarios. From top top bottom: LLJ is above, in the middle, or below the rotor swept area, and (b) corresponding streamwise turbulence intensity $\sigma_u = u'/u_{\text{hub}}$ at hub-height, where u' represents the fluctuating streamwise velocity.

3.2. Axial velocity

Figure 3 shows the axial velocity in the rotor plane for the three cases under consideration. Note that the axial velocity is normalized with the inlet velocity at hub-height. The figure shows that the velocity in the rotor plane is reduced compared to the incoming flow at hub-height. Due to the root vortices, the velocity near the root is higher than in the rest of the rotor plane [38]. A comparison of the axial velocity distribution in the rotor plane for the different scenarios clearly reveals the effect of the LLJ height. When $z_{\text{jet}} > z_h$, the turbine operates in a positive shear region with a higher velocity above the hub and lower velocity below. Consequently, the axial velocity is weaker below the hub and stronger above. When $z_{\text{jet}} \approx z_h$ there is positive shear below the hub and negative shear above the hub, the axial velocity distribution in the rotor plane is symmetric around hub-height. When the $z_{\text{jet}} < z_h$, the axial velocity is weaker above the hub and stronger below the hub. In this case, the turbine operates in the negative shear region with a lower velocity above and higher velocity below the turbine hub. This asymmetry in axial velocity distribution has an impact on the aerodynamic blade loads.

Effect of LLJ on aerodynamic blade loading using LES

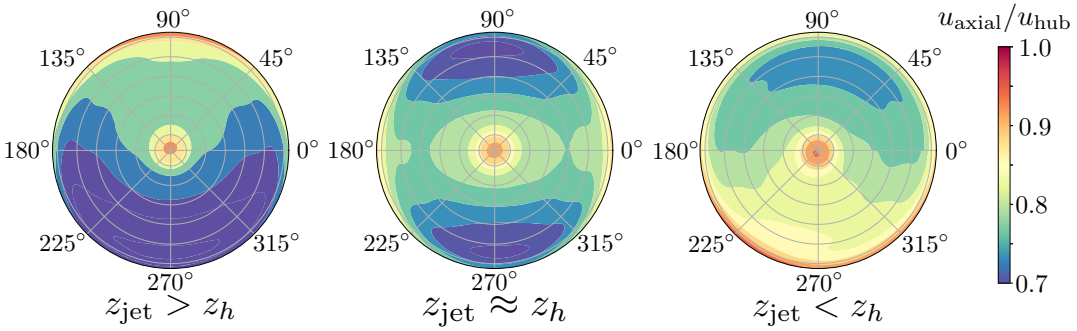

Figure 3: Time-averaged axial velocity u_{axial} at different azimuthal angles. The results are normalized with the inlet velocity at hub-height u_{hub}.

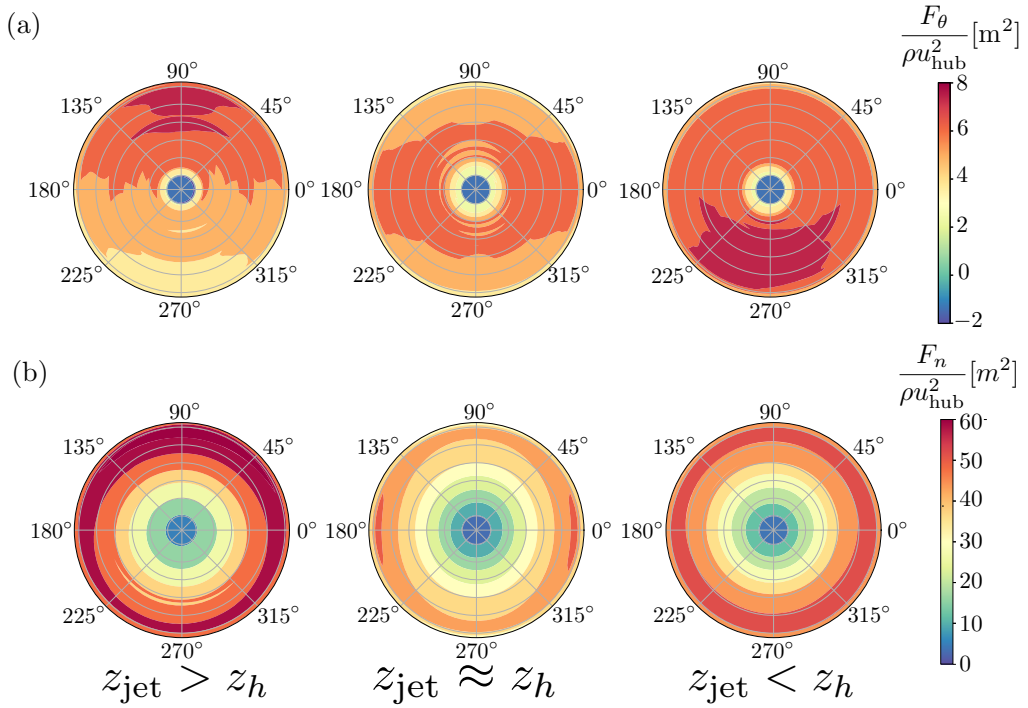

Figure 4: Azimuthal variation of (a) Tangential force F_θ and (b) Axial force F_n. The forces are normalized using hub-height velocity of the inlet flow field u_{hub}.

3.3. External aerodynamic blade loading

Figures 4(a) and (b) show the azimuthal variation of the normalized external aerodynamic blade loads, i.e. the tangential and axial forces, respectively. In a wind turbine, the rotor hub moments are large when there is an imbalance between the aerodynamic loads on the left and right or upper and lower parts of the rotor [31]. Furthermore, a large azimuthal variation in the normalized forces generally represents cyclical loading and causes higher fatigue on the blades. An important observation from Fig. 4(a) and (b) is that the blade loading is increased by the LLJ. We also observe that

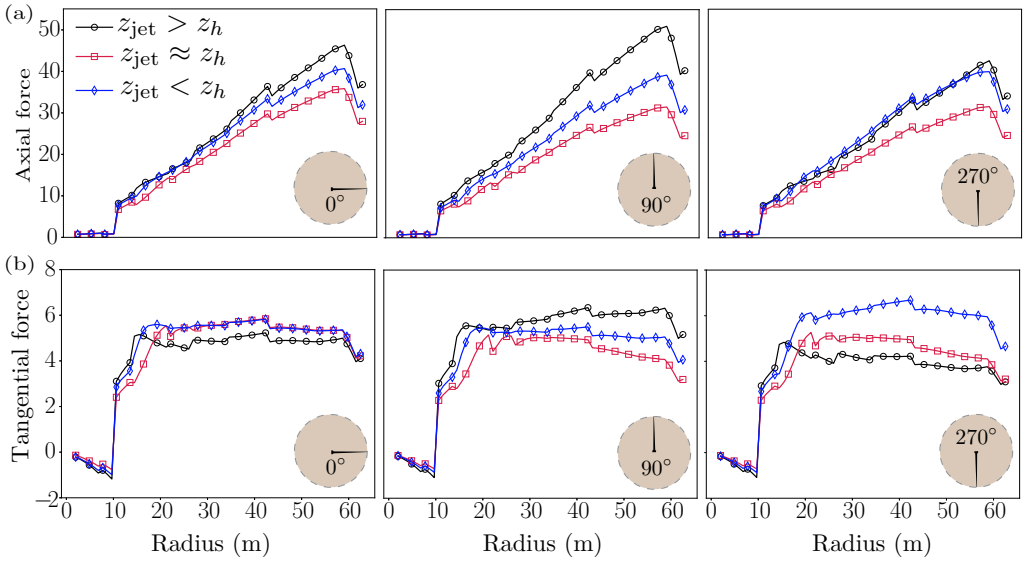

Figure 5: (a) Axial force ($F_n/\rho u_{\text{hub}}^2$ [m^2]) and (b) Tangential force ($F_\theta/\rho u_{\text{hub}}^2$ [m^2]). The black lines represent the position of the actuator line.

the LLJ shear, both positive and negative, causes a significant azimuthal variation in the aerodynamic forces. When $z_{\text{jet}} > z_h$ the rotor is subjected to large tangential and axial loads when the blade is at 90° due to the interaction of the turbine blades with the LLJ. When $z_{\text{jet}} \approx z_h$, the blade loading is highest at horizontal positions (0° and 180°), and lowest at vertical positions of the blade (90° and 270°). In contrast, when $z_{\text{jet}} < z_h$, the blade loads are nearly constant between 0° and 180° but increase as the blade interacts with the jet. Figure 4 convincingly shows that the presence of an LLJ causes an imbalance in the external aerodynamic blade loading and moments.

To further analyze the blade loading, we plot the radial variation of the axial and tangential forces for azimuthal angles of 0°, 90°, and 270° in Fig. 5(a) and (b), respectively. 0° indicates that the blade is in a horizontal position, and 90° and 270° represent the upward and downward positions of the blade (as indicated in the figure), respectively. All the forces are normalized using the inlet velocity at hub-height. Figure 5(a) shows that the normalized axial force for the case with $z_{\text{jet}} > z_h$ (LLJ is above hub-height) is higher than the other two cases when the blade angle is 90°. In addition, the tangential force increases approximately by 50% as the blade changes from downward (270°) to upward (90°) position. This clearly shows that the positive shear of the LLJ induces the highest cyclical loads. In contrast, when the LLJ is in the middle or below the rotor swept area, the variation in the forces between the horizontal and vertical positions is just 10 to 20% indicating limited azimuthal load variations. However, it is worth noting that when the LLJ is in the middle of the rotor swept area, the radial variation in the forces is higher for vertical positions of the blade. This indicates that longer blades will be subjected to higher cyclical loads. In Fig. 5(b) we observe that the tangential forces on the blades are highest at 270° when the LLJ is below the rotor

swept area. This indicates that both positive and negative shear of the LLJ induce strong cyclical loading.

4. Conclusions

We performed LES of a wind turbine in the presence of a LLJ using actuator line modeling and studied the effect of the LLJ height on the turbine wake vortices, external aerodynamic blade loading, and wake turbulence. We considered three different scenarios, wherein the LLJ is above, in the middle, and below the turbine rotor swept area. Flow visualizations reveal that the tip and root vortices are very stable when the jet is below the rotor swept area as the turbine is then operating in a thermally stratified region with negligible atmospheric turbulence. When the LLJ is above the turbines, the tip and root vortices quickly become unstable and break down due to atmospheric turbulence. We also found that the turbulence intensity in the near wake is highest when the LLJ is above the turbine rotor area and lowest when the LLJ is below the turbine. We find that the presence of LLJ gives rise to different axial velocity distributions in the rotor plane corresponding to the LLJ shear, which leads to variation in the aerodynamic forces.

Gutierrez *et al.* [22] report the turbine blades are subjected to cyclical aerodynamic loads that negatively impact the turbine that during an LLJ event. Our results agree with this and show that the LLJ increases the external aerodynamic blade loading. Additional loads due to LLJs create imbalances causing increased rotor moments. Furthermore, we find that the positive shear of the LLJ causes the highest azimuthal variation in the aerodynamic loads. At the 90° position, the tip of the blade interacts with the LLJ maximum and is therefore subjected to the highest loads, causing significant rotor hub moments, which is detrimental to the wind turbine. For the scenarios considered in the study, azimuthal variation in loads reduces when the LLJ is below or in the middle of the rotor swept area, with least azimuthal variation in the latter scenario. However further studies with additional turbine height-to-diameter ratios are necessary to generalize the results to a wider parameter range.

Acknowledgments

This work is part of the Shell-NWO/FOM-initiative Computational sciences for energy research of Shell and Chemical Sciences, Earth and Live Sciences, Physical Sciences, FOM, and STW. We also acknowledge PRACE for awarding us access to MareNostrum 4 based in Spain under PRACE project number 2020225335.

References

[1] N. Troldborg, J. N. Sørensen, and R. Mikkelsen, *Actuator line simulation of wake of wind turbine operating in turbulent inflow*, J. Phys. Conf. Ser. **75**, 012063 (2007).

[2] L. Chamorro and F. Porté-Agel, *A Wind-Tunnel Investigation of Wind-Turbine Wakes: Boundary-Layer Turbulence Effects*, Boundary-Layer Meteorol. **132**, 129 (2009).
[3] J. M. S. Bartl, F. V. Mühle, J. Schottler, L. R. Sætran, J. Peinke, S. M. Adaramola, and M. Holling, *Wind tunnel experiments on wind turbine wakes in yaw: effects of inflow turbulence and shear*, Wind Energy Science **3**, 329 (2018).
[4] E. Kleusberg, S. Benard, and D. S. Henningson, *Tip-vortex breakdown of wind turbines subject to shear*, Wind Energy **22**, 1789 (2019).
[5] A. Smedman, U. Högström, and H. Bergström, *Low level jets - A decisive factor for off-shore wind energy siting in the Baltic Sea*, Wind Engineering **20**, 137 (1996).
[6] P. C. Kalverla, J. B. Duncan Jr., G.-J. Steeneveld, and A. A. M. Holtslag, *Low-level jets over the North Sea based on ERA5 and observations: together they do better*, Wind Energy Science **4**, 193 (2019).
[7] P. Baas, F. C. Bosveld, H. K. Baltink, and A. A. M. Holtslag, *A climatology of nocturnal low-level jets at Cabauw*, J. Appl. Meteorol. Climatol. **48**, 1627 (2009).
[8] R. M. Banta, *Stable-boundary-layer regimes from the perspective of the low-level jet*, Acta Geophysica **56**, 58 (2008).
[9] R. W. Arritt, T. D. Rink, M. Segal, D. P. Todey, C. A. Clark, M. J. Mitchell, and K. M. Labas, *The Great Plains low-level jet during the warm season of 1993*, Mon. Weather Rev. **125**, 2176 (1997).
[10] R. M. Banta, Y. L. Pichugina, N. D. Kelley, B. Jonkman, and W. A. Brewer, *Doppler lidar measurements of the Great Plains low-level jet: Applications to wind energy*, IOP Conf. Ser.: Earth Environ. Sci. **1**, 012020 (2008).
[11] J. B. Duncan, *Observational analyses of the North Sea low-level jet* (TNO, Petten, Netherlands, 2018).
[12] W. Gutierrez, G. Araya, S. Basu, A. Ruiz-Columbie, and L. Castillo, *Toward understanding low level jet climatology over West Texas and its impact on wind energy*, J. Phys. Conf. Ser. **524**, 012008 (2014).
[13] J. A. Aird, R. J. Barthelmie, T. J. Shepherd, and S. C. Pryor, *WRF-Simulated springtime low-level jets over Iowa: Implications for Wind Energy*, J. Phys. Conf. Ser. **1618**, 062020 (2020).
[14] B. J. Vanderwende, J. K. Lundquist, M. E. Rhodes, E. S. Takle, and S. L. Irvin, *Observing and simulating the Summertime low-level jet in central Iowa*, Monthly Weather Review **143**, 2319 (2015).
[15] P. C. Kalverla, Ph.D. thesis, University of Wageningen, 2019.
[16] R. J. Barthelmie, T. J. Shepherd, J. A. Aird, and S. C. Pryor, *Power and wind shear implications of large wind turbine scenarios in the US Central Plains*, Energies **13**, 4269 (2020).
[17] H. Lu and F. Porté-Agel, *Large-eddy simulation of a very large wind farm in a stable atmospheric boundary layer*, Phys. Fluids **23**, 065101 (2011).
[18] K. Bhaganagar and M. Debnath, *The effects of mean atmospheric forcings of the stable atmospheric boundary layer on wind turbine wake*, J. Renew. Sustain. Energy **7**, 013124 (2015).
[19] J. S. Na, E. Koo, E. K. Jin, R. Linn, S. C. Ko, D. Muñoz-Esparza, and J. S. Lee, *Large-eddy simulations of wind-farm wake characteristics associated with a low-level jet*, Wind Energy **21**, 163 (2018).
[20] S. N. Gadde and R. J. A. M. Stevens, *Interaction between low-level jets and wind farms in a stable atmospheric boundary layer*, Phys. Rev. Fluids **6**, 014603 (2021).
[21] S. N. Gadde and R. J. A. M. Stevens, *Effect of turbine-height on wind farm performance in the presence of a low-level jet*, J. Renew. Sustain. Energy **13**, 013305 (2021).
[22] W. Gutierrez, G. Araya, P. Kiliyanpilakkil, A. Ruiz-Columbie, M. Tutkun, and L. Castillo, *Structural impact assessment of low level jets over wind turbines*, J. Renew. Sustain. Energy **8**, 023308 (2016).
[23] W. Gutierrez, A. Ruiz-Columbie, M. Tutkun, and L. Castillo, *Impacts of the low-level jet's negative wind shear on the wind turbine*, Wind Energy Science **2**, 533 (2017).

[24] OpenFAST, https://www.nrel.gov/wind/nwtc/openfast.html, accessed: 2021-05-03.
[25] W. Gutierrez, A. Ruiz-Columbie, M. Tutkun, and L. Castillo, *The structural response of a wind turbine under operating conditions with a low-level jet*, Renew. Sust. Energ. Rev. **108**, 380 (2019).
[26] J. D. Albertson, Ph.D. thesis, University of California, 1996.
[27] M. Calaf, C. Meneveau, and J. Meyers, *Large eddy simulations of fully developed wind-turbine array boundary layers*, Phys. Fluids **22**, 015110 (2010).
[28] M. Zhang, M. G. Arendshorst, and R. J. A. M. Stevens, *Large eddy simulations of the effect of vertical staggering in extended wind farms*, Wind Energy **22**, 189 (2019).
[29] M. Abkar and P. Moin, *Large eddy simulation of thermally stratified atmospheric boundary layer flow using a minimum dissipation model*, Boundary-Layer Meteorol. **165**, 405 (2017).
[30] J. N. Sørensen and W. Z. Shen, *Computation of wind turbine wakes using combined Navier-Stokes actuator-line Methodology*, In Proceedings of European Wind Energy Conference EWEC 99, Nice, France: 1999; 156– 159. 156 (1999).
[31] N. Troldborg, J. N. Sørensen, and R. Mikkelsen, *Numerical simulations of wake characteristics of a wind turbine in uniform inflow*, Wind Energy **13**, 86 (2010).
[32] R. J. A. M. Stevens, L. A. Martínez-Tossas, and C. Meneveau, *Comparison of wind farm large eddy simulations using actuator disk and actuator line models with wind tunnel experiments*, Renewable Energy **116**, 470 (2018).
[33] R. J. Beare, M. K. Macvean, A. A. M. Holtslag, J. Cuxart, I. Esau, J.-C. Golaz, M. A. Jimenez, M. Khairoutdinov, B. Kosović, D. Lewellen, T. S. Lund, J. K. Lundquist, A. Mccabe, A. F. Moene, Y. Noh, S. Raasch, and P. Sullivan, *An intercomparison of large eddy simulations of the stable boundary layer*, Boundary-Layer Meteorol. **118**, 247 (2006).
[34] R. J. A. M. Stevens, J. Graham, and C. Meneveau, *A concurrent precursor inflow method for large eddy simulations and applications to finite length wind farms*, Renewable Energy **68**, 46 (2014).
[35] N. Troldborg, G. C. Larsen, H. A. Madsen, K. S. Hansen, J. N. Sørensen, and R. Mikkelsen, *Numerical simulations of wake interaction between two wind turbines at various inflow conditions*, Wind Energy **14**, 859 (2011).
[36] K. S. Hansen, R. J. Barthelmie, L. E. Jensen, and A. Sommer, *The impact of turbulence intensity and atmospheric stability on power deficits due to wind turbine wakes at Horns Rev wind farm*, Wind Energy **15**, 183 (2012).
[37] R. J. Barthelmie, K. Hansen, S. T. Frandsen, O. Rathmann, J. G. Schepers, W. Schlez, J. Phillips, K. Rados, A. Zervos, E. S. Politis, and P. K. Chaviaropoulos, *Modelling and Measuring Flow and Wind Turbine Wakes in Large Wind Farms Offshore*, Wind Energy **12**, 431 (2009).
[38] S. Ivanell, J. N. Sørensen, and D. Henningson, *Numerical Computations of Wind Turbine Wakes*, In Wind Energy, edited by J. Peinke, P. Schaumann, and S. Barth 259 (2007).